


# Growth of magnesium diboride thin films on boron buffered Si and silicon-on-insulator substrates by hybrid physical chemical vapor deposition

Wenura K Withanage<sup>1</sup> , Sashank V Penmatsa<sup>1</sup>, Narendra Acharya<sup>1</sup>, Thomas Melbourne<sup>1</sup>, D Cunnane<sup>2</sup>, B S Karasik<sup>2</sup> and X X Xi<sup>1</sup>

<sup>1</sup>Department of Physics, Temple University, Philadelphia, PA 19122, United States of America

<sup>2</sup>Jet Propulsion Laboratory, California Institute of Technology, Pasadena, CA 91109, United States of America

E-mail: [tue76590@temple.edu](mailto:tue76590@temple.edu)

Received 2 April 2018, revised 9 May 2018

Accepted for publication 22 May 2018

Published 11 June 2018



## Abstract

We report on the growth of high quality  $\text{MgB}_2$  thin films on silicon and silicon-on-insulator substrates by hybrid physical chemical vapor deposition. A boron buffer layer was deposited on all sides of the Si substrate to prevent the reaction of Mg vapor and Si. Ar ion milling at a low angle of  $1^\circ$  was used to reduce the roughness of the boron buffer layer before the  $\text{MgB}_2$  growth. An Ar ion milling at low angle of  $1^\circ$  was also applied to the  $\text{MgB}_2$  surface to reduce its roughness. The resultant  $\text{MgB}_2$  films showed excellent superconducting properties and a smooth surface. The process produces thin  $\text{MgB}_2$  films suitable for waveguide-based superconducting hot electron bolometers and other  $\text{MgB}_2$ -based electronic devices.

Keywords: magnesium diboride, thin films, HEB mixers

(Some figures may appear in colour only in the online journal)

## 1. Introduction

Superconducting hot electron bolometers (HEBs) have become the state of the art technology for high-resolution spectroscopy at terahertz frequencies, and the current HEB technology is based on niobium nitride (NbN) thin films [1–3]. The superconducting transition temperature ( $T_c$ ) of the ultrathin NbN films used in HEB mixers is close to 11 K [4], and this has limited the operational temperature of the NbN based HEB mixers to around 4.2 K. Owing to its high  $T_c$  ( $\sim 39$  K) [5] and short electron–phonon interaction time (few picoseconds) [6], and fast phonon escape rate,  $\text{MgB}_2$  has become a promising candidate for wideband HEBs with good sensitivity and higher operational temperatures. To ensure large intermediate frequency (IF) bandwidth of HEBs, typically  $\text{MgB}_2$  thin films with thickness below 20 nm are preferred [7, 8]. These ultrathin films ensure fast thermal relaxation in the film due to the high phonon escape

rate from film to the substrate. Quasioptical  $\text{MgB}_2$  based HEBs prepared on semi-insulating (THz-transparent) 6H-SiC have been characterized by Cunnane *et al* at 0.6, 1.6, 2.5 THz [7], and 4.3 THz (unpublished) showing a high IF bandwidth and high operational temperatures. Additionally, Novoselov *et al* have reported low noise  $\text{MgB}_2$  HEB mixers with an 11 GHz bandwidth with low noise temperature [8]. To match the impedance between antenna and the HEB, films with normal state sheet resistance above  $50 \Omega/\text{square}$  are preferred. However, the  $\text{MgB}_2$  films on SiC show low normal state resistivity [9].

Recently, waveguide-based NbN HEB mixers at 2.7 THz [10] and 4.7 THz [11] have been reported. These waveguide-based NbN HEB mixers use ultrathin NbN films on Si membranes with  $2\text{--}3 \mu\text{m}$  thickness and they offer several benefits:

- Horn antennas used with waveguide-based mixers provide a beam of better quality than hyperhemispherical (or elliptical) lenses used in quasioptical THz mixers.

- In mixer arrays, pixels can be closely spaced allowing for more compact design and better utilization of the local oscillator power.
- Modular array architecture can be implemented allowing for adding more pixels to the already existing mixer array.

The dielectric membrane substrate becomes absolutely necessary here as it eliminates the leakage of the radiation power through the waveguide sidewalls [12, 13]. Fabrication of devices on membranes is a well-established process. It is based on the use of a silicon-on-insulator (SOI) substrate [14, 15]. Membrane based  $\text{MgB}_2$  HEB mixers have not been reported, mainly due to the difficulty of growing high quality  $\text{MgB}_2$  thin films on Si or SOI substrates.

The main objective of this work is to develop a growth process for high quality  $\text{MgB}_2$  thin and ultrathin films on Si and SOI substrates for the development of membrane based  $\text{MgB}_2$  HEB mixers. However, a broader interest from various applications for high quality superconducting  $\text{MgB}_2$  thin films on Si substrates is expected, as Si is widely used in electronic devices and can be micro-machined.

In this paper, we describe the growth of  $\text{MgB}_2$  thin films on boron buffered silicon and SOI substrates, which showed high transition temperatures and high critical current densities. Furthermore, we show that the roughness of the  $\text{MgB}_2$  films can be reduced by Ar ion milling of the boron buffer layer and the  $\text{MgB}_2$  films, making them suitable for HEB device applications.

## 2. Experimental details

Hybrid physical chemical vapor deposition (HPCVD) [9, 16] is an effective method of growing  $\text{MgB}_2$  thin films. In the HPCVD technique, the  $\text{MgB}_2$  film growth takes place at  $\sim 700^\circ\text{C}$  (above the melting temperature of Mg) and the melting of the Mg pellets around the substrate ensures high Mg vapor pressure during the  $\text{MgB}_2$  growth, which is important to preserve the  $\text{MgB}_2$  phase stability [17]. However, Mg vapor and Si readily react to form  $\text{Mg}_2\text{Si}$  alloy at elevated temperatures and this process was observed already at  $\sim 550^\circ\text{C}$ .

There are two options to prevent the alloy formation between the Si substrate and the Mg vapor: (i) reduction of the growth temperature below the  $\text{Mg}_2\text{Si}$  alloy formation temperature and (ii) incorporation of a suitable buffer layer. One may also grow  $\text{MgB}_2$  on the top of the alloy layer [18]. Lee *et al* have grown  $\text{MgB}_2$  films on  $\text{Al}_2\text{O}_3$  buffered Si substrates at low temperatures ( $500^\circ\text{C}$ – $600^\circ\text{C}$ ) using HPCVD [19]. However, the films grown at lower temperatures showed rough surfaces making it difficult to use for micron-size device fabrication, and some alloy formation was observed even with the low deposition temperature and the  $\text{Al}_2\text{O}_3$  buffer layer. As mentioned earlier, high Mg vapor pressure is the key requirement for growing high quality  $\text{MgB}_2$  thin films using the HPCVD method. Therefore, it requires an incorporation of a buffer layer that can

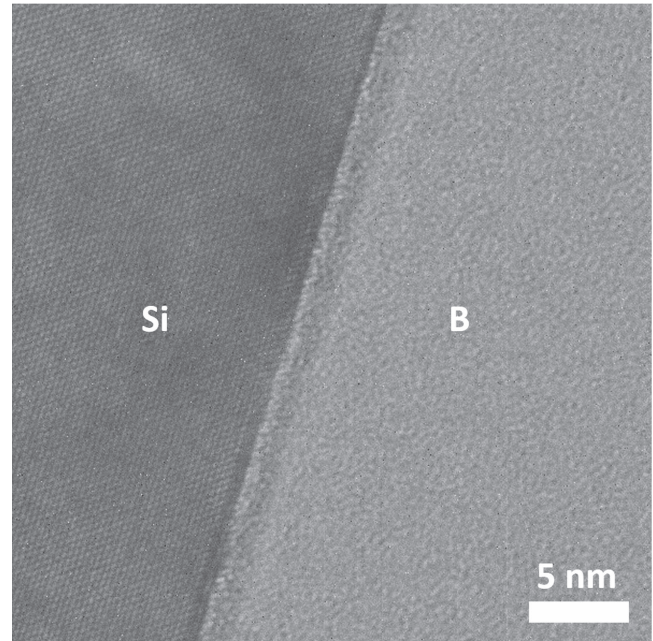


**Figure 1.** TEM cross-section image of the B–Si interface of an  $\text{MgB}_2$  film grown on a B buffered Si substrate.

successfully prevent the alloy formation between Mg and Si even above the Mg melting temperature. A  $\sim 220$  nm thick boron buffer layer was found to successfully prevent the reaction between Mg and Si at  $\sim 700^\circ\text{C}$ .

In this work, high resistivity float zone growth Si (100) substrates were used. A boron layer was deposited on the both sides of the Si substrate by CVD with  $\text{B}_2\text{H}_6$  as the precursor gas in a large HPCVD reactor without using Mg pieces. Growth of the boron layer was initiated with the introduction of 20 sccm flow of 5%  $\text{B}_2\text{H}_6$  in  $\text{H}_2$  gas to the HPCVD chamber at 40 Torr of  $\text{H}_2$  background pressure at  $470^\circ\text{C}$  for 5 min. This process resulted in a  $\sim 220$  nm thick boron layer which was sufficient to prevent the reaction between Mg and Si at high temperatures. The boron layer thickness can be controlled by adjusting the  $\text{B}_2\text{H}_6$  flow rate or the deposition time. The  $\text{MgB}_2$  film deposition was carried out similarly to the standard HPCVD method. To determine the thickness and the growth rate of  $\text{MgB}_2$  films, a step was created on the film by wet etching with aqua regia and the step height was measured using atomic force microscopy (AFM). The boron layer showed resistance to the etching with aqua regia.  $\text{MgB}_2$  growth rate was used for the thickness calculation for the films grown with similar conditions.

Ar ion milling was carried out by using an Int'lVac ion milling system with a 200 mA ion beam current and 400 V acceleration voltage at an angle of  $1^\circ$ . Resistivity versus temperature ( $RT$ ) dependencies and critical current density ( $J_c$ ) at different temperatures were measured for different film thicknesses using the four-point method. For these measurements,  $5 \times 100 \mu\text{m}^2$  and  $10 \times 200 \mu\text{m}^2$  bridges were fabricated using photolithography. Cross-sectional studies of samples were carried out by using a JEOL



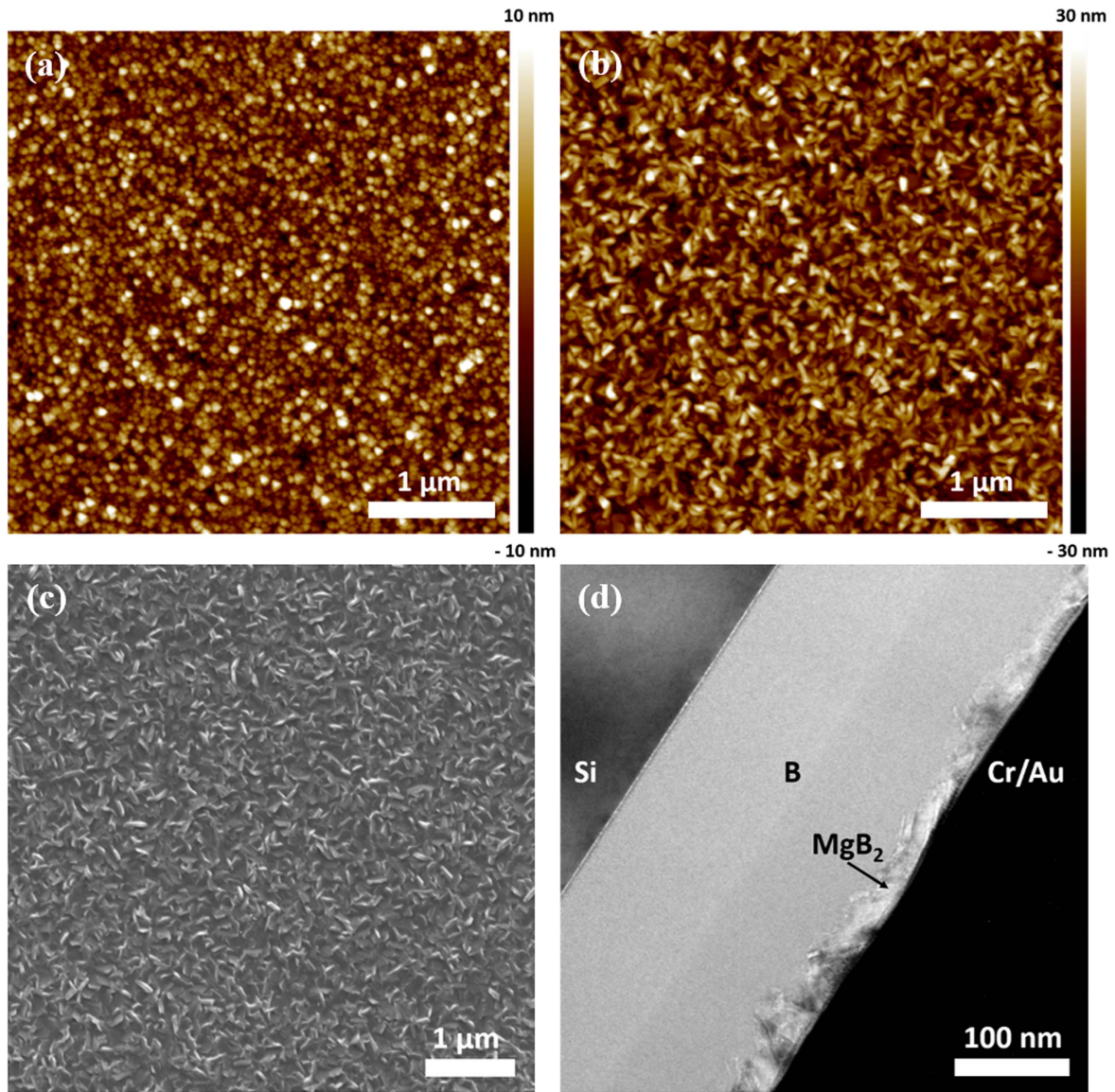


**Figure 2.** (a) AFM image of the B surface of a B buffered Si substrate. (b) AFM image of a 24 nm MgB<sub>2</sub> thin film grown on B buffered Si. (c) SEM image of a 24 nm MgB<sub>2</sub> thin film grown on B buffered Si. (d) TEM cross-section image of an MgB<sub>2</sub> film grown on B buffered Si.

JEM2100 transmission electron microscope (TEM). The TEM samples were prepared by using an FEI Strata DB235 dual beam focused ion beam (FIB) system. Surface morphology of the samples was studied by using a 470 FEI Quanta FEG scanning electron microscope (SEM) and a Veeco Icon AFM.

### 3. Results and discussions

Figure 1 shows a TEM cross-section image of the B–Si interface of a B buffered Si substrate after the MgB<sub>2</sub> deposition. For HEB applications, a concern with the boron buffer layer on Si was the inter-diffusion of B and Si to form a conductive layer at the interface, which can absorb terahertz radiation and reduce the performance of the

device. The TEM image shows a sharp interface between the B and Si layers with no indication of the B and Si inter-diffusion. While crystal planes can be observed in the Si substrate, no crystal planes are visible in the B layer due to the amorphous nature of the B layer. No Mg–Si alloy is seen in the TEM image, demonstrating the effectiveness of the B buffer layer in preventing the Mg–Si alloy formation during the MgB<sub>2</sub> film growth. However, occasionally we observe some alloy spots formation on MgB<sub>2</sub> films. This can be as a result of B uncoated areas on the substrate or any scratches occurring in the B coated substrate handling process.

An AFM image of the B buffer layer surface is shown in figure 2(a). The root mean square (rms) roughness ( $R_q$ ) of the boron layer was around  $\sim 3.5$  nm in a  $25 \mu\text{m}^2$  area. The topography of a 24 nm MgB<sub>2</sub> film grown on B buffered Si

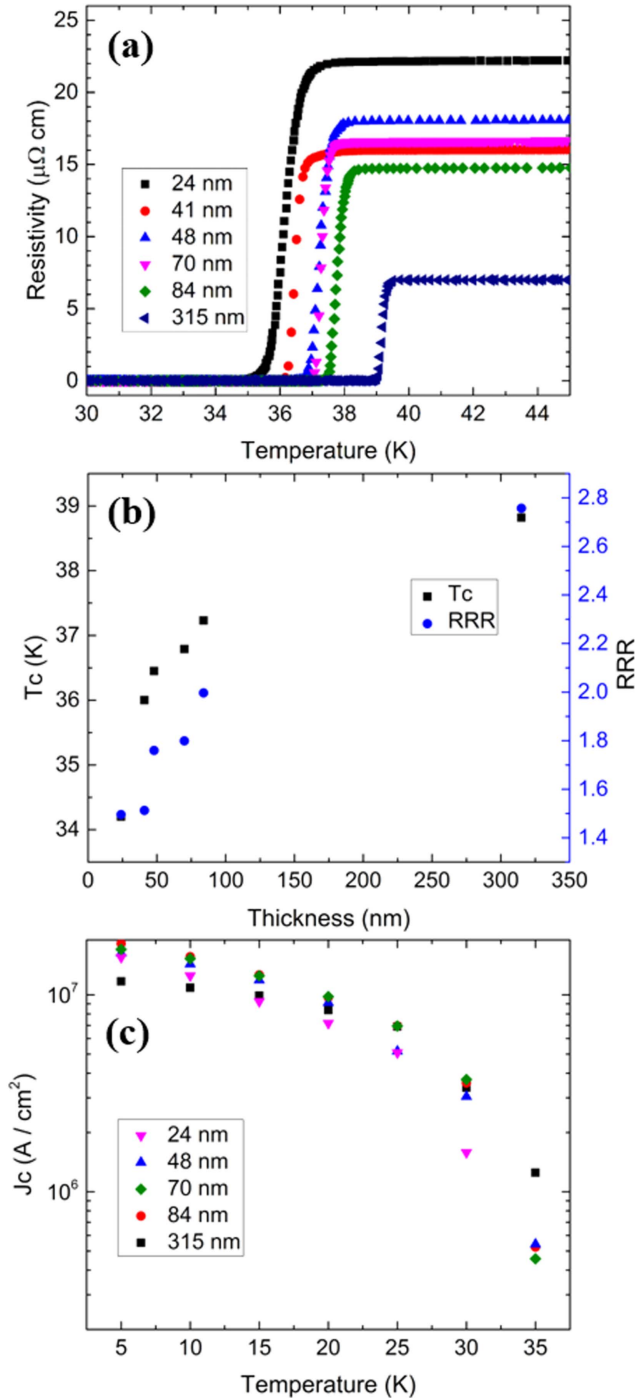


**Figure 3.** (a)  $R$  versus  $T$  curves of  $\text{MgB}_2$  films grown on B buffered Si near  $T_c$ . (b)  $T_c$  and RRR of the  $\text{MgB}_2$  films grown on B buffered Si. (c)  $J_c$  versus  $T$  curves of  $\text{MgB}_2$  films grown on B buffered Si.

substrate is shown in figure 2(b), measured by AFM, and in figure 2(c), measured by SEM. From both images, it can be clearly seen that the  $\text{MgB}_2$  film is polycrystalline, consistent with our previous observations of  $\text{MgB}_2$  films grown on amorphous substrates. The roughness of the film in figure 2(b) is  $R_q \sim 9.3\text{ nm}$ . It should be noted that the growth rate ( $\sim 24\text{ nm min}^{-1}$ ) of  $\text{MgB}_2$  on the B buffered Si substrate was significantly higher than the epitaxial  $c$ -axis

oriented  $\text{MgB}_2$  growth rate on single-crystalline 6H-SiC substrate ( $\sim 15\text{ nm min}^{-1}$ ) under the same growth conditions. This may be attributed to the tilted hexagonal grains oriented randomly in the polycrystalline films. This also increases the roughness of the films significantly. The rms roughness in a  $25\text{ }\mu\text{m}^2$  area ranges between 8 nm and 55 nm for  $\text{MgB}_2$  films with thicknesses ranging from 24 nm to 315 nm, respectively. A TEM cross-section image of an  $\text{MgB}_2/\text{B}/\text{Si}$  sample is shown in figure 2(d). A Cr/Au layer deposited on top of the  $\text{MgB}_2$  layer was for the TEM sample preparation using FIB. It can be seen that the interface between the B layer and the  $\text{MgB}_2$  film is very rough. The  $\text{MgB}_2$  layer surface was Ar ion milled prior to the TEM sample preparation, thus a smooth  $\text{MgB}_2$  surface was observed.

The  $R$  versus  $T$  curves near  $T_c$  for films with different thicknesses can be seen in figure 3(a). The  $T_c$  of the films decreases with the decreasing film thickness, similar to the thickness dependence observed in epitaxial  $\text{MgB}_2$  films grown on SiC substrate [20]. Figure 3(b) shows the  $T_c$  (squares) and the residual resistivity ratio [RRR =  $R(300\text{ K})/R(50\text{ K})$ ] (circles) with respect to the thickness of the films. The highest  $T_c$  observed was 39 K for the 315 nm thick film and the lowest  $T_c$  observed was 35 K for the 24 nm thick film. The normal state resistivity of the films varied between 22 to  $35\text{ }\mu\Omega\text{ cm}$  with decreasing film thickness from 315 to 24 nm. The normal state resistivity values of the  $\text{MgB}_2$  films grown on B buffered Si substrates are significantly higher than epitaxial  $\text{MgB}_2$  films grown on SiC [20]. This is beneficial to the HEB mixer allowing for improved radio-frequency impedance matching of the devices to antenna or waveguide circuit. The RRR of the films were reduced substantially to  $\sim 2$  from that of the epitaxial thin films. Both the increase in the normal state resistivity and the lower RRR may be attributed to the polycrystalline nature of the film and the less grain connectivity compared to an epitaxial film. The temperature dependence of  $J_c$  for different film thicknesses is shown in figure 3(c). High zero-field  $J_c$  values above  $10^7\text{ A cm}^{-2}$  at 5 K are observed in the films of all thicknesses. The 315 nm film shows slightly lower  $J_c$  compared to the thinner films. However, the enhanced roughness of the films adds a large uncertainty to the thickness measurement of the  $\text{MgB}_2$  films. This can result in a significant error in the resistivity and critical current density calculations.

The HEB and other device fabrications require smooth superconducting films. A major issue encountered in the  $\text{MgB}_2$  film growth on B buffered Si substrates was the roughness of the boron layer, which led to the increased roughness of the  $\text{MgB}_2$  films. Acharya *et al* [20] have reported production of ultrathin  $\text{MgB}_2$  films with Ar ion milling of as-grown  $\text{MgB}_2$  films at  $10^\circ$  and  $15^\circ$  with minimal damage to the superconductivity. In this work, Ar ion milling at a low angle of  $1^\circ$  was used to reduce the roughness of the B surface and the  $\text{MgB}_2$  layer. The B surface was milled for 30 min. At the  $1^\circ$  angle, the milling rate of B is negligibly



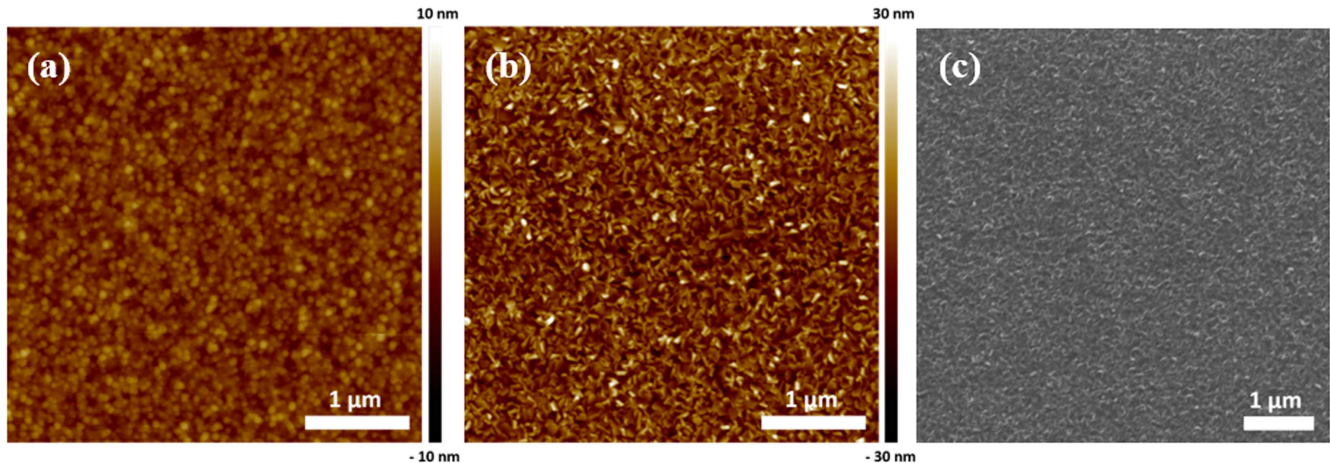


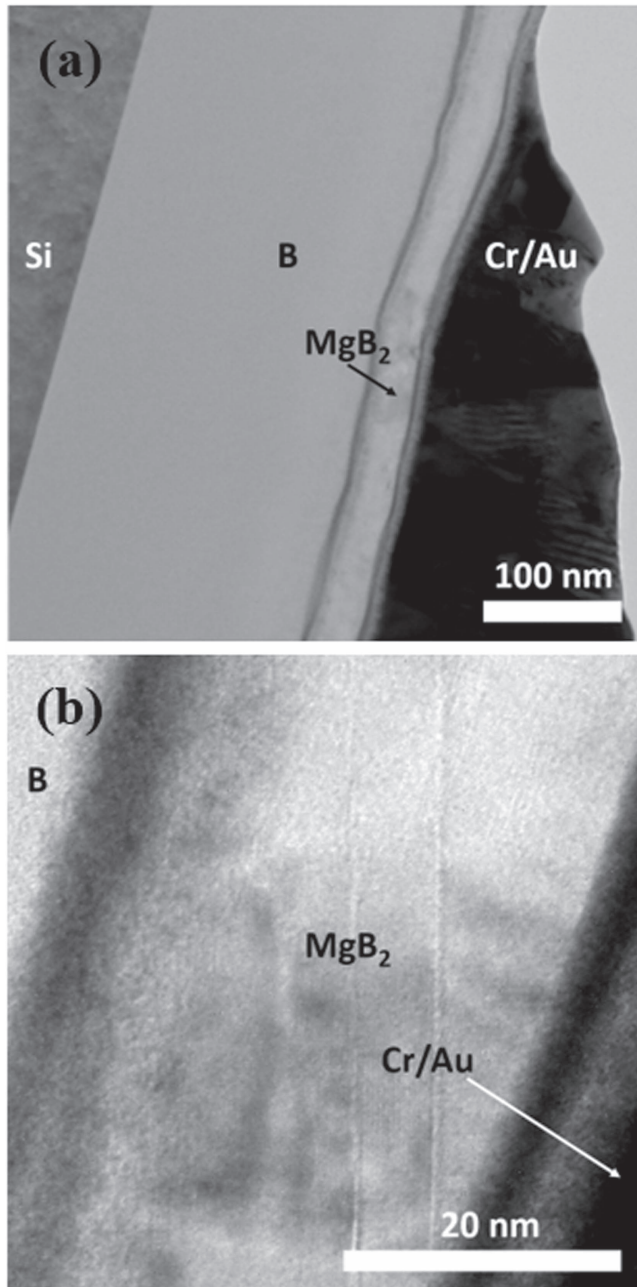
**Figure 4.** (a) AFM image of the B surface of an ion milled B buffered Si substrate. (b) AFM image of a 30 nm MgB<sub>2</sub> thin film grown on ion milled B buffered Si. (c) SEM image of a nm MgB<sub>2</sub> thin film grown on ion milled B buffered Si.

low ( $\sim 0.15 \text{ nm min}^{-1}$ ). The same low angle Ar ion milling was used to reduce the surface roughness of the MgB<sub>2</sub> films with different milling times and the milling rate was  $\sim 0.5 \text{ nm min}^{-1}$ .

Figure 4(a) shows an AFM image of an Ar ion milled B surface. It can be clearly seen that the surface roughness has decreased compared to the as-grown B surface (figure 2(a)) and  $R_q$  was decreased to  $\sim 2 \text{ nm}$  from  $3.5 \text{ nm}$  of as-grown boron surface. The topography of a 30 nm MgB<sub>2</sub> film grown on ion milled B surface is shown in figure 4(b), measured by AFM, and in figure 4(c), measured by SEM. The surface roughness of the films has improved and the grain size has decreased noticeably in comparison to an MgB<sub>2</sub> film of the comparable thickness grown on B buffered Si without milling shown in figures 2(b) and (c). Figure 5(a) shows a TEM image of an MgB<sub>2</sub> film on an ion milled B surface on Si. From this image, a smooth albeit wavy interface between the B and MgB<sub>2</sub> film can be seen, as the result of the B buffer layer roughness reduction with Ar ion milling. A zoomed in TEM image at the boundary of the MgB<sub>2</sub> film is shown in figure 5(b). In both TEM images, two dark layers on the either side of the MgB<sub>2</sub> film can be seen, possibly due to a slight defocus as the result of the electron beam being aligned with the crystal planes in the Si substrate.

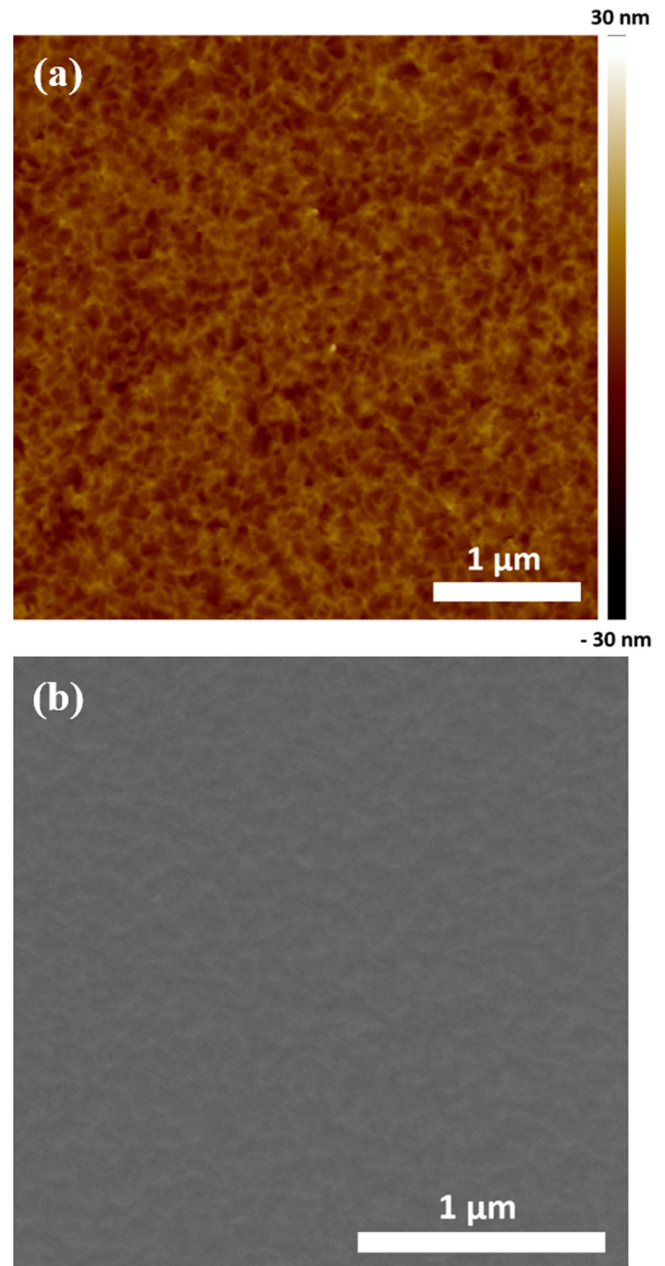
Ar ion milling was used on such MgB<sub>2</sub> films to further reduce their surface roughness. Figures 6(a) and (b) show the MgB<sub>2</sub> surface after 8 min of ion milling of a 30 nm MgB<sub>2</sub> film grown on ion milled B surface on Si. The tilted grain structure observed in figure 4(b) is no longer visible after the ion milling. The Ar ions removed the sharp edges of the tilted grains, thus reducing the surface roughness of the films. The 30 nm film showed a roughness  $R_q \sim 6.4 \text{ nm}$  in a  $25 \mu\text{m}^2$  area before the ion milling, which was reduced to  $R_q \sim 2.6 \text{ nm}$  after the ion milling. The ion milling at a rate of  $\sim 0.5 \text{ nm min}^{-1}$  also reduced the film thickness, with a final thickness of the film estimated to be  $26 \text{ nm}$ . The roughness of  $R_q \sim 2.6 \text{ nm}$  is comparable to similarly thick epitaxial MgB<sub>2</sub> thin films grown on SiC substrates.

Figure 7(a) shows the  $R$  versus  $T$  curves of as-grown (solid symbols) and ion milled (open symbols) MgB<sub>2</sub> films of different thicknesses grown on the ion milled B buffer layer on Si. However, the films grown on milled B surface showed reduced  $T_c$  compared to similarly thick MgB<sub>2</sub> films grown on as-grown B surface (figures 3(a) and (b)). Similar behavior was also observed in terms of the grain size in these two sets of films. The ion milling of the MgB<sub>2</sub> films reduces their  $T_c$  along with their thickness. Figure 7(b) shows the thickness dependence of  $T_c$  (squares) and RRR (circles) of as-grown (solid symbols) and ion milled (open symbols) MgB<sub>2</sub> films grown on the ion milled B buffer layer on Si. RRR values of the as-grown films on milled B surface has slightly decreased compared to similarly thick films grown on as-grown B surface (figure 3 (b)), while the normal state resistivity has increased noticeably (figure 3(a)). Due to the change in the film roughness, the accuracy of the thickness measurement degrades and, therefore, the resistivity values before and after the ion milling become difficult to compare. A significant difference in RRR values were not observed between the ion milled and the as-grown films. Figure 7(c) shows the temperature dependence of  $J_c$  for the as-grown (solid symbols) and ion milled (open symbols) MgB<sub>2</sub> films of different thicknesses on the ion milled B buffer layer on Si. Both ion milled and as-grown MgB<sub>2</sub> films show a slight reduction of  $J_c$  in comparison with films grown on the as-grown boron surface. This may be attributed to the change in the boron layer surface during the Ar ion milling. An amorphous boron surface layer may affect the nucleation of the MgB<sub>2</sub> film, leading to changes in the grain structure and the superconducting properties. MgB<sub>2</sub> ‘flowers’ like growth structure have been reported by Seong *et al* [21] on amorphous boron layers. Significant degradation due to the Ar ion milling of the MgB<sub>2</sub> film surface is not expected as previous studies showed excellent superconducting properties in Ar ion milled epitaxial MgB<sub>2</sub> films grown on SiC substrates [20].



**Figure 5.** (a) TEM cross-section image of an  $\text{MgB}_2$  film grown on ion milled B buffered Si. (b) Zoomed in cross-section image of the  $\text{MgB}_2$  layer.

Figure 8(a) shows an AFM image of a 20 nm thick  $\text{MgB}_2$  film grown on B buffered SOI substrate. Film shows polycrystalline nature with roughness  $R_q$  of 12 nm. Normalized resistance versus temperature curves of 20 and 40 nm films are shown in the figure 8(b). These resistance versus temperature measurements were carried out on unpatterned  $\text{MgB}_2$  films on irregularly shaped SOI substrates and the resistance of the films was normalized to the resistance at 40 K. From figure 8(b), one can see that the films on SOI showed similar transition temperatures to the films grown on B buffered Si substrates (figures 2(a) and (b)). Hence, the same ion milling technique described above



**Figure 6.** (a) AFM image of the surface of an ion milled  $\text{MgB}_2$  film on ion milled B buffered Si. (b) SEM surface of an ion milled  $\text{MgB}_2$  film on ion milled B buffered Si.

can be applied to further reduce the film roughness of the  $\text{MgB}_2$  films on SOI substrates.

#### 4. Conclusions

In summary, we have successfully developed a new  $\text{MgB}_2$  thin film growth process on Si substrates by incorporating a  $\sim 220$  nm B buffer layer. The B buffer layer was shown to successfully prevent the Mg–Si reaction even above 700 °C and no diffusion of B and Si layers was observed at the B–Si interface. With the same technique, polycrystalline  $\text{MgB}_2$



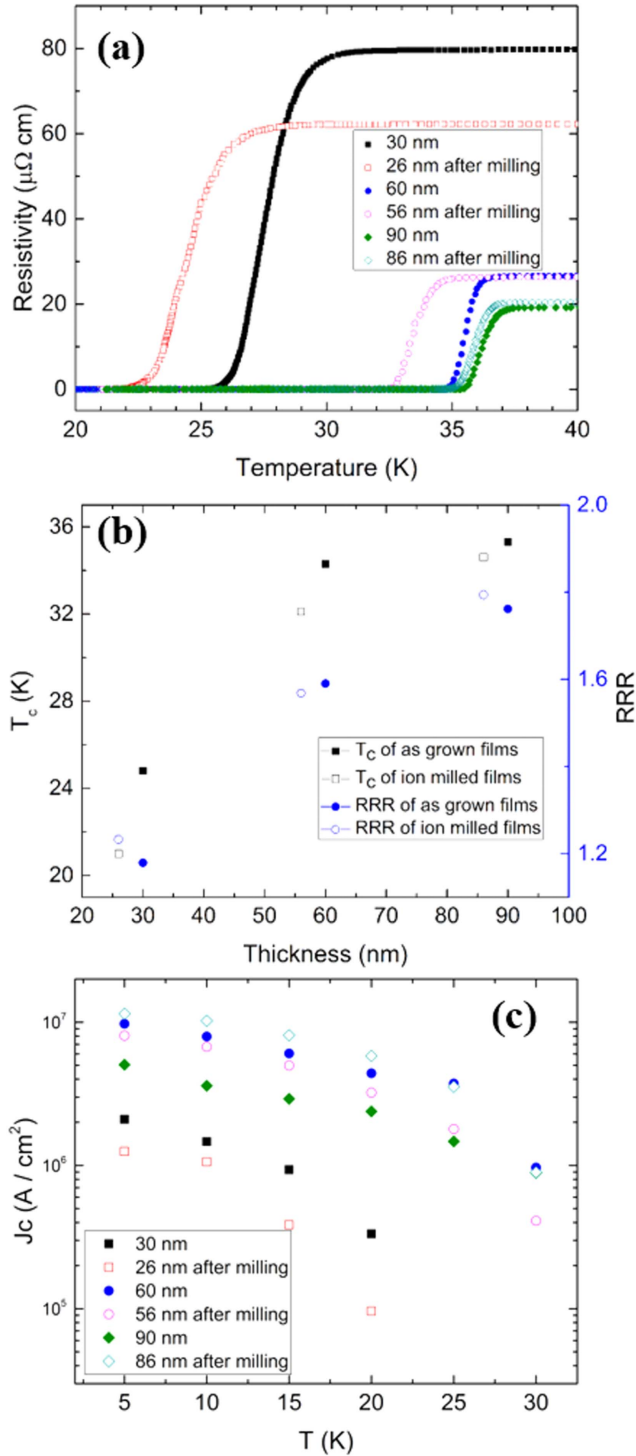


**Figure 7.** (a)  $R$  versus  $T$  curves of ion milled and as-grown MgB<sub>2</sub> films grown on ion milled B buffered Si near  $T_c$ . (b)  $T_c$  and RRR of the ion milled and as-grown MgB<sub>2</sub> films grown on ion milled B buffered Si. (c)  $J_c$  versus  $T$  curves of the ion milled and as-grown MgB<sub>2</sub> films grown on ion milled B buffered Si.

films were deposited on SOI substrates. Milling both the B buffer and the MgB<sub>2</sub> film with Ar ions at a low angle  $\sim 1^\circ$  allowed for a significant improvement of the film surface smoothness. The MgB<sub>2</sub> thin films thus grown showed high  $T_c$  (22–39 K) and high  $J_c$  ( $10^6$ – $10^7 \text{ A cm}^{-2}$  at 5 K) along with a small surface roughness ( $R_q \sim 2.6 \text{ nm}$ ) that is suitable for the

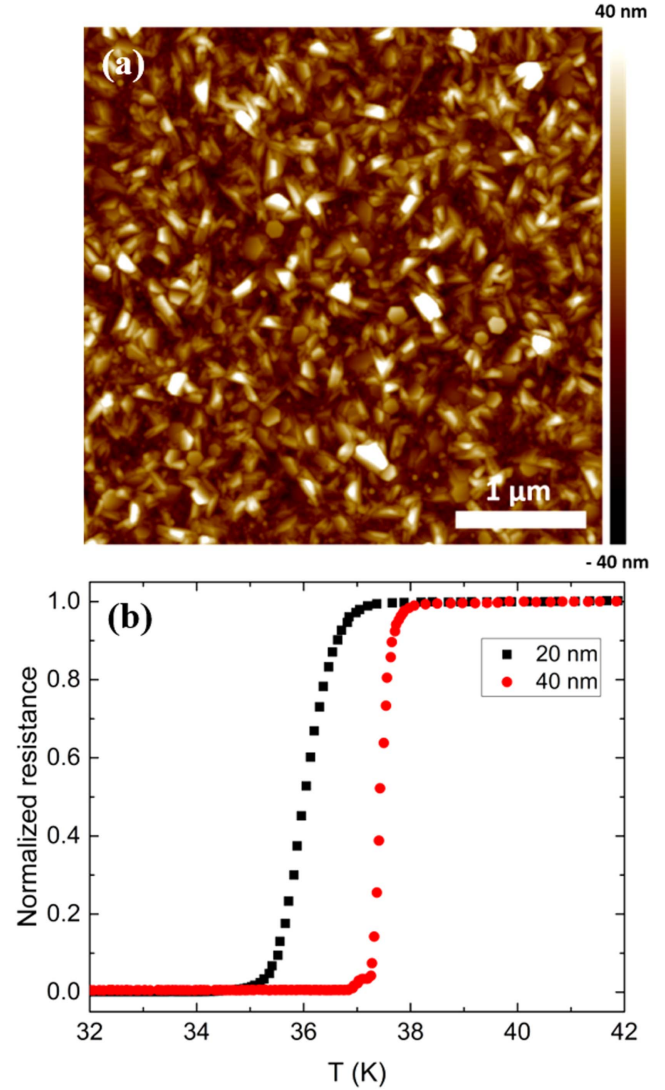


**Figure 8.** (a) AFM image of an MgB<sub>2</sub> film on B buffered SOI substrate. (b)  $R$  versus  $T$  curves of MgB<sub>2</sub> films grown on B buffered SOI substrates near  $T_c$ .

device fabrication. Polycrystalline MgB<sub>2</sub> thin films on boron buffered Si showed increased normal state resistivity and this will ease the fabrication of well impedance-matched HEB devices. The superconducting properties of these films are comparable to those grown on other amorphous substrates. Given the widespread use of Si in electronic circuits, this process may help to expand the use of MgB<sub>2</sub> devices in various applications.

## Acknowledgments

The work carried out at Temple University was supported by the NASA's Astrophysics Research and Analysis Program through a contract from JPL. This work made use of the CoE-NIC facility at Temple University. The CoE-NIC is based on DoD DURIP Award N0014-12-1-0777 from the Office of Naval Research and is sponsored by the College of

Engineering, Temple University. The work at the Jet Propulsion Laboratory, California Institute of Technology, was carried out under a contract with the National Aeronautics and Space Administration. We would like to thank Dr Craig Johnson at Drexel University for his support with TEM cross-section images.

## ORCID iDs

Wenura K Withanage  <https://orcid.org/0000-0003-1350-9423>

## References

- [1] Shurakov A, Lobanov Y and Goltsman G 2016 Superconducting hot-electron bolometer: from the discovery of hot-electron phenomena to practical applications *Supercond. Sci. Technol.* **29** 023001
- [2] Kroug M, Cherednichenko S, Merkel H, Kollberg E, Voronov B, Gol'tsman G, Huebers H W and Richter H 2001 NbN hot electron bolometric mixers for terahertz receivers *IEEE Trans. Appl. Supercond.* **11** 962–5
- [3] Hajenius M, Baselmans J J A, Baryshev A, Gao J R, Klapwijk T M, Kooi J W, Jellema W and Yang Z Q 2006 Full characterization and analysis of a terahertz heterodyne receiver based on a NbN hot electron bolometer *J. Appl. Phys.* **100** 074507
- [4] Kang L *et al* 2011 Suppression of superconductivity in epitaxial NbN ultrathin films *J. Appl. Phys.* **109** 033908
- [5] Nagamatsu J, Nakagawa N, Muranaka T, Zenitani Y and Akimitsu J 2001 Superconductivity at 39 K in magnesium diboride *Nature* **410** 63–4
- [6] Xu Y, Khafizov M, Satrapinsky L, Kus P, Plecenik A, Karpinski J, Jun J, Kazakov S M and Sobolewski R 2004 Picosecond dynamics of the superconducting state in MgB<sub>2</sub> *Physica C* **408–410** 90–2
- [7] Cunnane D, Kawamura J H, Wolak M A, Acharya N, Tan T, Xi X X and Karasik B S 2015 Characterization of MgB<sub>2</sub> superconducting hot electron bolometers *IEEE Trans. Appl. Supercond.* **25** 2300206
- [8] Novoselov E and Cherednichenko S 2017 Low noise terahertz MgB<sub>2</sub> hot-electron bolometer mixers with an 11 GHz bandwidth *Appl. Phys. Lett.* **110** 032601
- [9] Wolak M A, Acharya N, Tan T, Cunnane D, Karasik B S and Xi X X 2015 Fabrication and characterization of ultrathin MgB<sub>2</sub> films for hot-electron bolometer applications *IEEE Trans. Appl. Supercond.* **25** 7500905
- [10] Boussaha F M, Kawamura J H, Stern J A, Skalare A and White V 2012 A low noise 2.7 THz waveguide-based superconducting mixer *IEEE Trans. THz Sci. Technol.* **2** 284–9
- [11] Buchel D *et al* 2015 4.7 THz superconducting hot electron bolometer waveguide mixer *IEEE Trans. THz Sci. Technol.* **5** 207–14
- [12] Rebeiz G M 1992 Millimeter-wave and terahertz integrated-circuit antennas *Proc. IEEE* **80** 1748–70
- [13] Alexopoulos N G, Katehi P B and Rutledge D B 1983 Substrate optimization for integrated-circuit antennas *IEEE Trans. Microw. Theory Tech.* **31** 550–7
- [14] Kaul A B, Bumble B, Lee K A, LeDuc H G, Rice F and Zmuidzinas J 2004 Fabrication of wide-IF 200–300 GHz superconductor-insulator-superconductor mixers with suspended metal beam leads formed on silicon-on-insulator *J. Vac. Sci. Technol. B* **22** 2417–22
- [15] Barker N S, Bauwens M, Lichtenberger A and Weikle R 2017 Silicon-on-Insulator substrates as a micromachining platform for advanced terahertz circuits *Proc. IEEE* **105** 1105–20
- [16] Xi X X *et al* 2007 MgB<sub>2</sub> thin films by hybrid physical-chemical vapor deposition *Physica C* **456** 22–37
- [17] Liu Z K, Schlom D G, Li Q and Xi X X 2001 Thermodynamics of the Mg-B system: Implications for the deposition of MgB<sub>2</sub> thin films *Appl. Phys. Lett.* **78** 3678–80
- [18] Withanage W K, Xi X X, Nassiri A, Lee N, Wolak M A, Tan T, Welander P B, Franzi M, Tantawi S and Kustom R L 2017 Growth of magnesium diboride films on 2 inch diameter copper discs by hybrid physical-chemical vapor deposition *Supercond. Sci. Technol.* **30** 045001
- [19] Lee T G, Park S W, Seong W K, Huh J Y, Jung S G, Lee B K, An K S and Kang W N 2008 Growth of MgB<sub>2</sub> thin films on alumina-buffered Si substrates by using hybrid physical-chemical vapor deposition method *Physica C* **468** 1888–91
- [20] Acharya N, Wolak M A, Tan T, Lee N, Lang A C, Taheri M, Cunnane D, Karasik B S and Xi X X 2016 MgB<sub>2</sub> ultrathin films fabricated by hybrid physical-chemical vapor deposition and ion milling *APL Mater.* **4** 086114
- [21] Seong W K, Ranot M, Lee J Y, Yang C W, Lee J H, Oh Y H, Ahn J P and Kang W N 2016 Superconducting MgB<sub>2</sub> flowers: growth mechanism and their superconducting properties *Supercond. Sci. Technol.* **29** 045015